Supplementary Information

The structural basis of Edc3- and Scd6-mediated activation of the Dcp1:Dcp2 mRNA decapping complex

Simon A. Fromm, Vincent Truffault, Julia Kamenz, Joerg E. Braun, Niklas A. Hoffmann, Elisa Izaurralde, Remco Sprangers

Figure S1

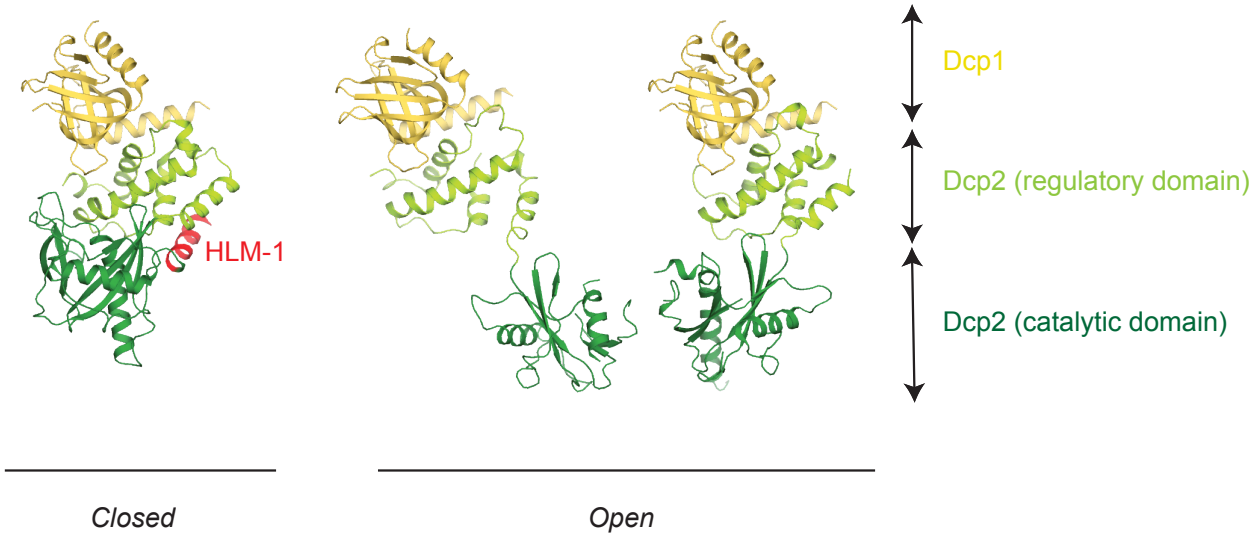

Figure S1: Structural plasticity in the decapping complex

The different orientations the Dcp2 catalytic domain adopts with respect to Dcp1 and the Dcp2 regulatory domain in three independent crystal structures. Left and middle: the two crystal forms for the Dcp1:Dcp2 complex (pdb-code: 2QKM), right: crystal structure of the free Dcp2 enzyme (pdb-code 2A6T) modeled on the Dcp1:Dcp2 complex structure. A large degree of structural variation is possible between the regulatory and catalytic domains of Dcp2. Dcp1 is colored yellow, the Dcp2 regulatory domain light green, the Dcp2 catalytic domain dark green and the HLM-1 sequence in red. The structure on the left, where the Dcp2 regulatory and catalytic domains interact, is referred to as closed, the middle and right structures are considered to be in an open conformation. The HLM-1 sequence is not visible in the open conformations of the decapping complex.

Figure S2

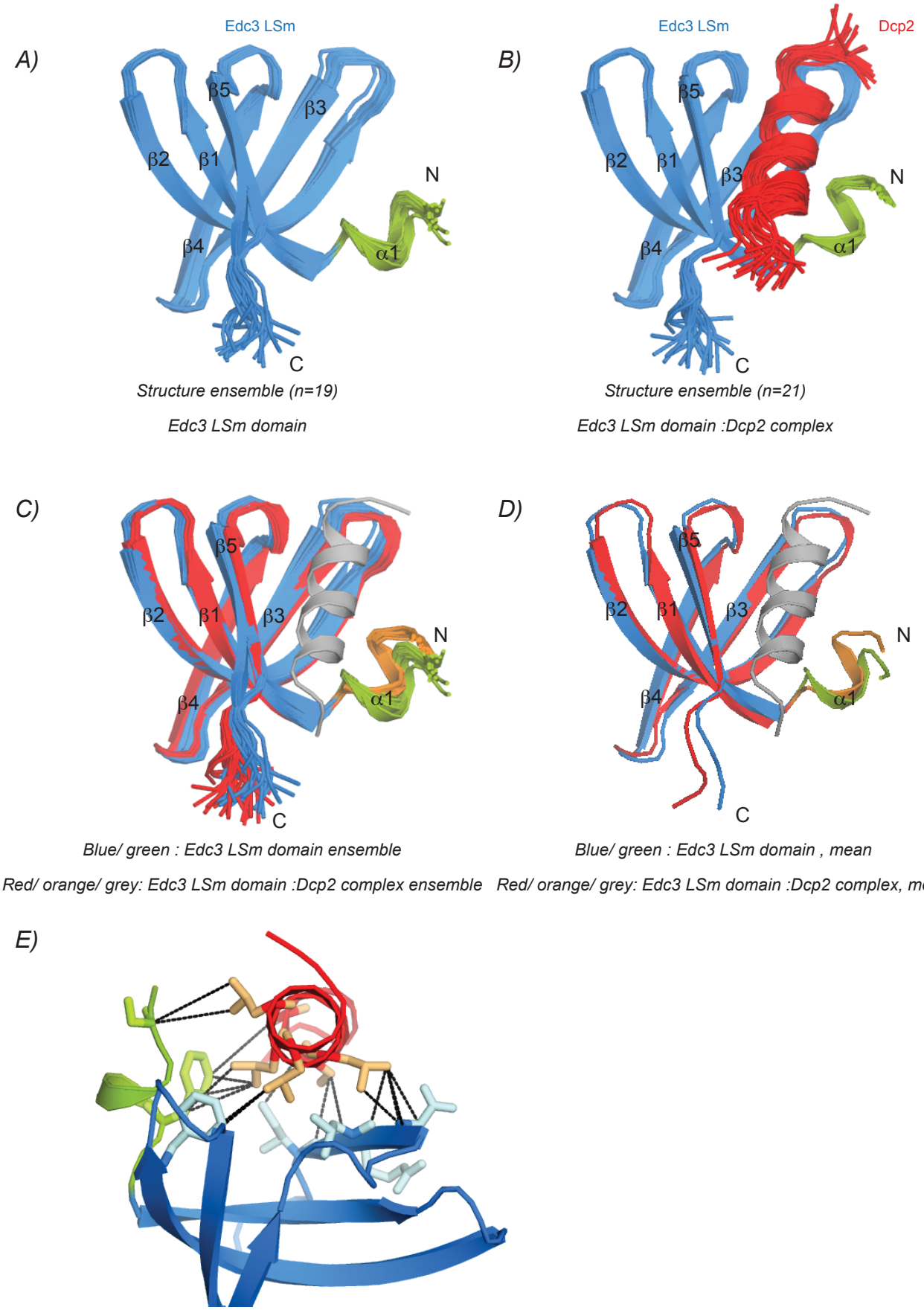

Structure ensemble (n=19)

Edc3 LSm domain

Structure ensemble (n=21)

Edc3 LSm domain :Dcp2 complex

Blue/ green : Edc3 LSm domain ensemble

Red/ orange/ grey: Edc3 LSm domain :Dcp2 complex ensemble

Blue/ green : Edc3 LSm domain , mean

Red/ orange/ grey: Edc3 LSm domain :Dcp2 complex, mean

Figure S2: The structures of the Edc3 LSm domain and the Edc3 LSm domain Dcp2 complex

The ensembles shown were obtained by superposition of the secondary structure elements of the individual structures (residues V3-L58 for Figures S2A, S2C and S2D; residues V3-L58 and A254-S267 for Figure S2B). An average structure (not shown) was calculated from the superimposed ensemble by averaging the coordinates of the individual structures. The rmsd (root mean square deviation) reported is the average rmsd of the individual members compared to the average structure (+/- standard deviation) (See also Table S1).

A. Ensemble of the 19 lowest energy structures (from a total of 50 calculated structures) of the free Edc3 LSm domain. The N-terminal helical turn is colored green for reference. The rmsd of the ensemble is: 0.26 +/- 0.13 Å (backbone) / 0.71 +/- 0.09 Å (heavy atoms).

B. Ensemble of the 21 lowest energy structures (from a total of 50 calculated structures) of the Edc3 LSm domain (blue, green) in complex with Dcp2 residues 257-266 (red). The rmsd of the ensemble is: 0 .54 +/- 0.14 Å (backbone) / 0.84 +/- 0.11 Å (heavy atoms).

C. Superposition of all 19 structures of the free Edc3 LSm domain (see panel A) and the 21 structures of the Edc3 LSm domain in complex with Dcp2 (panel B). The Edc3 LSm domains from the Edc3:Dcp2 structures are colored red and orange. The Dcp2 helix is shown in grey for reference and not included in the superposition of the ensemble. The rmds of the ensemble of 40 structures is: 0.44 +/- 0.08 Å (backbone) / 0.83 +/- 0.08 Å (heavy atoms).

D. Superposition of the average energy minimized structures of the Edc3 LSm domain (blue, green) and the Edc3 Lsm domain in complex with Dcp2 (red, orange, grey). The rmsd of the 2 structures is: 0.35 Å (backbone) / 0.51 Å (heavy atoms).

E. Structure of the Edc3 Lsm domain in complex with Dcp2. The NOE (nuclear Overhauser effect) contacts used in the structure calculations are marked with black lines. For clarity reasons, the protons are not shown and the NOE contacts are drawn between the heavy atoms that are directly bound to the protons for which the NOE contact was observed. In some cases, multiple NOEs (e.g. those resulting from the protons Hβ1 and Hβ2) are thus represented with a single line only.

Figure S3

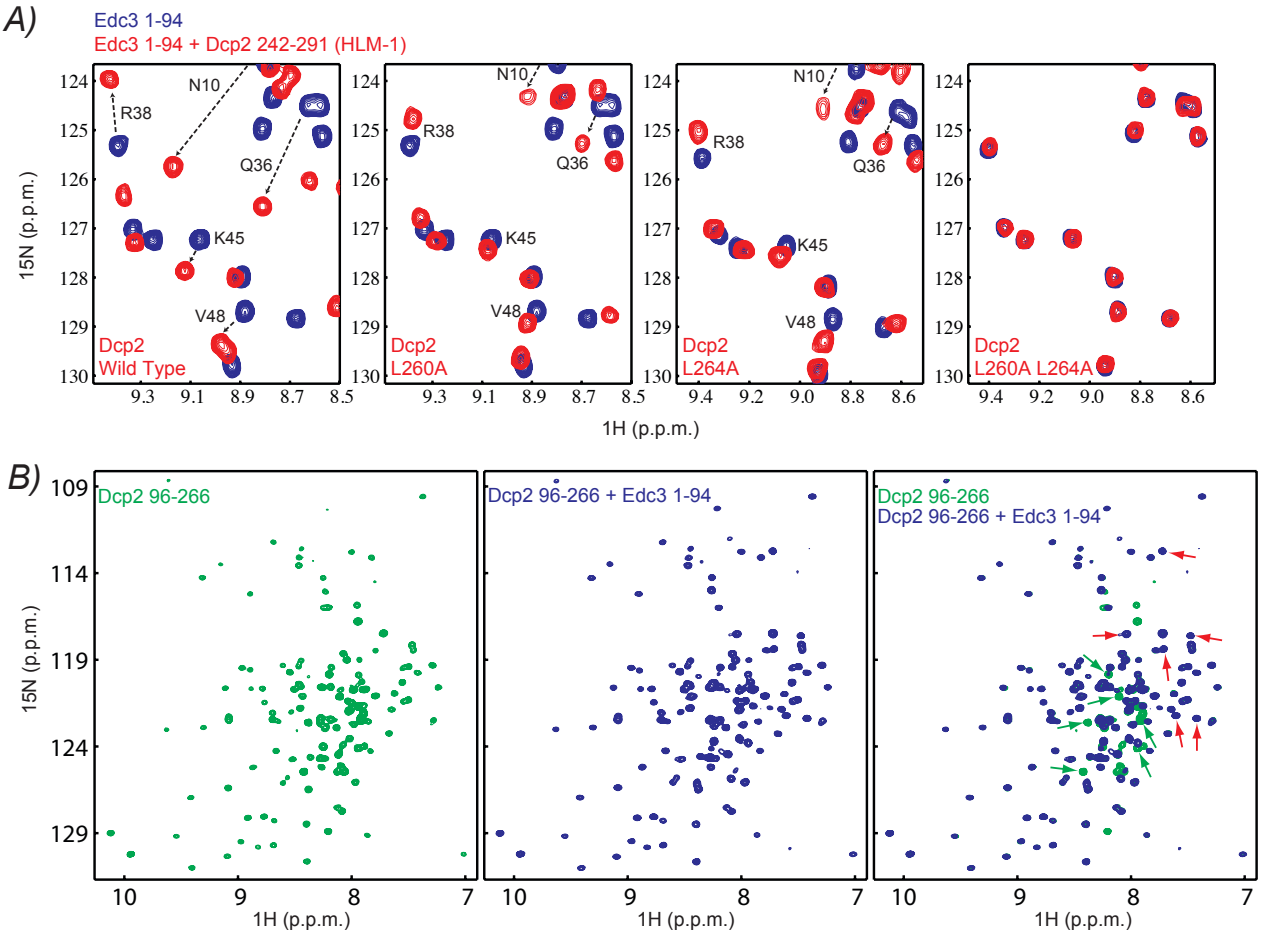

Figure S3: The LSm interaction motif is unfolded before interaction with Edc3

A. NMR spectra of the free Edc3 LSm domain (blue) in the presence (red) of the wild type HLM-1 (panel 1), HLM-1 where L260 is replaced with an alanine (panel 2), HLM-1 where L264 is replace with an alanine (panel 3), or HLM-1 where both L260 and L264 are replaced with alanines (panel 4). Replacing one leucine residue with an alanine reduces the extend of the chemical shift changes and thus the affinity between the Edc3 LSm domain and HLM-1. Replacing both leucine residues with alanine abolished the interaction completely.

B. 2D ^{1}H-^{15}N spectrum of Dcp2 residues 96-266 (catalytic domain plus the first LSm interacting motif, HLM-1), before (green, left) and after (blue, middle) addition of the Edc3 LSm domain. Upon addition of the Edc3 LSm domain, peaks that are located in a spectral region indicative of an unfolded backbone (green arrows) move to spectral regions that indicate secondary structure (red arrows, right spectrum). This indicates the formation of the HLM-1 helix in solution upon Edc3 addition. Due to the lack of the regulatory domain in the Dcp2 96-266 construct, the HLM-1 helix

is in a disordered conformation like in the open form of the decapping complex. In that regard, the Dcp2 96-266 construct resembles the open conformation of the Dcp1:Dcp2 complex.

Figure S4

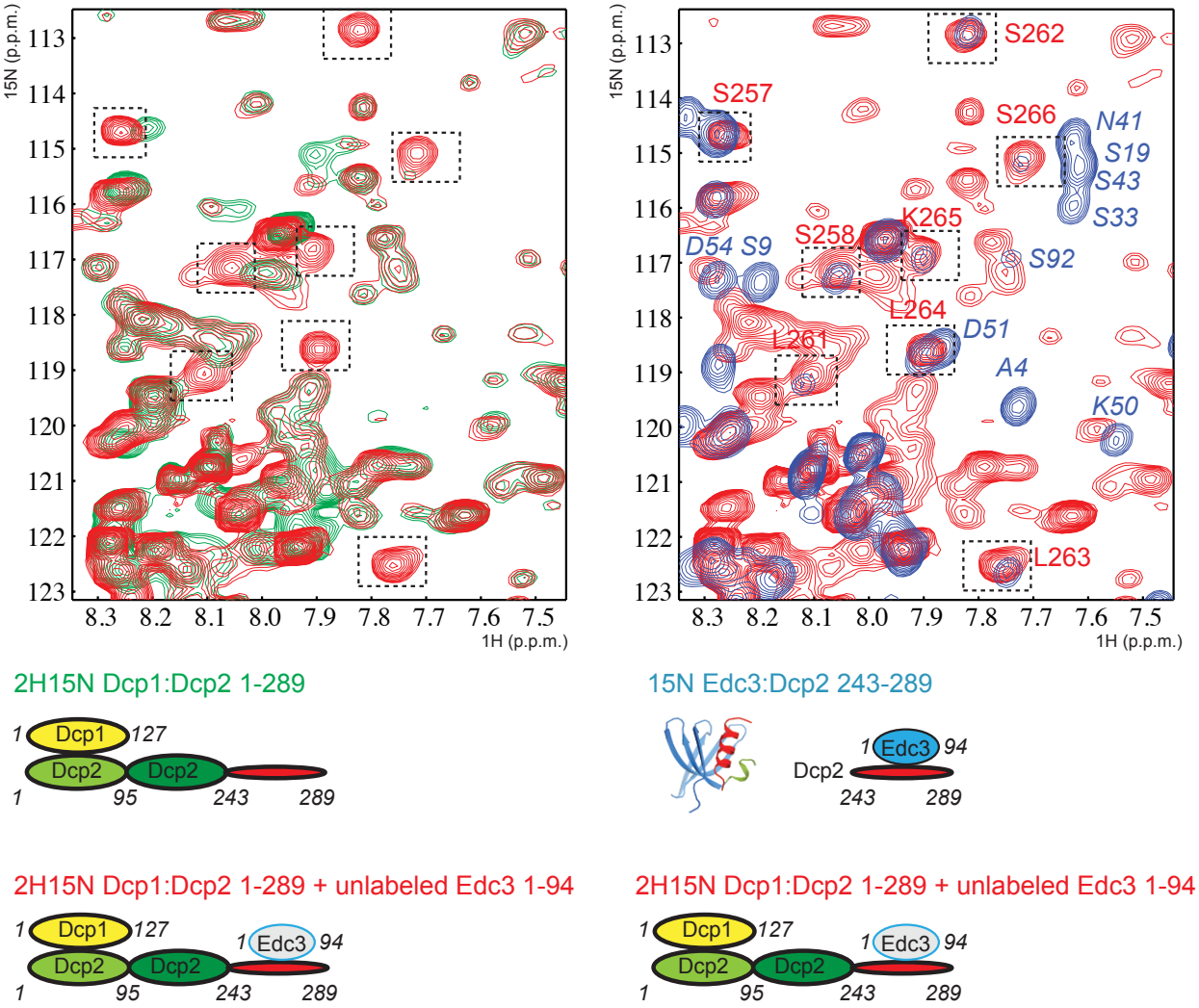

Figure S4: The Edc3-Dcp2 structure is the same in isolation and in the context of the complete decapping complex

Top left: Overlay of a region of a 2D ^{1}H-^{15}N spectrum of active Dcp1:Dcp2 residues 1-289 (regulatory domain, catalytic domain plus the LSm interacting motif) without (green) and with the (NMR inactive) Edc3 LSm domain (red). Upon addition of the LSm domain, a set of peaks appears in the Dcp1:Dcp2 spectrum (red, boxes), that indicates the formation of a structured region in the complex.

Top right: Overlay of the 2D ^{1}H-^{15}N spectrum of NMR active Dcp1:Dcp2 (residues 1-289) in complex with Edc3 (red, same spectrum as in A) and a ^{1}H-^{15}N spectrum of the complex of NMR active Edc3 LSm domain with Dcp2 residues 242 to 291 (blue). The resonances in the blue spectrum (both the Edc3 LSm domain and Dcp2 are NMR active) were fully assigned and correspond to the structure of the Edc3:Dcp2 complex we solved here. Assignments for the LSm

domain in the complex are indicated with blue labels, assignments for Dcp2 in the complex are indicated with red labels. Resonance frequencies for Dcp2 residues 242-291 are identical in the minimal Edc3:Dcp2 complex and in the complete Dcp1:Dcp2:Edc3 complex (boxed regions are the same in A and in B). This indicates that the Dcp2 helix is folded identically in the context of the isolated Edc3 LSm domain (structure) and in the context of the full Dcp1:Dcp2 Edc3 bound decapping complex. Cartoons of the complexes are indicated at the bottom, NMR inactive components are colored in gray; Dcp1 in yellow, Dcp2 in green, the LSm interaction motif in red and Edc3 in blue.

Figure S5

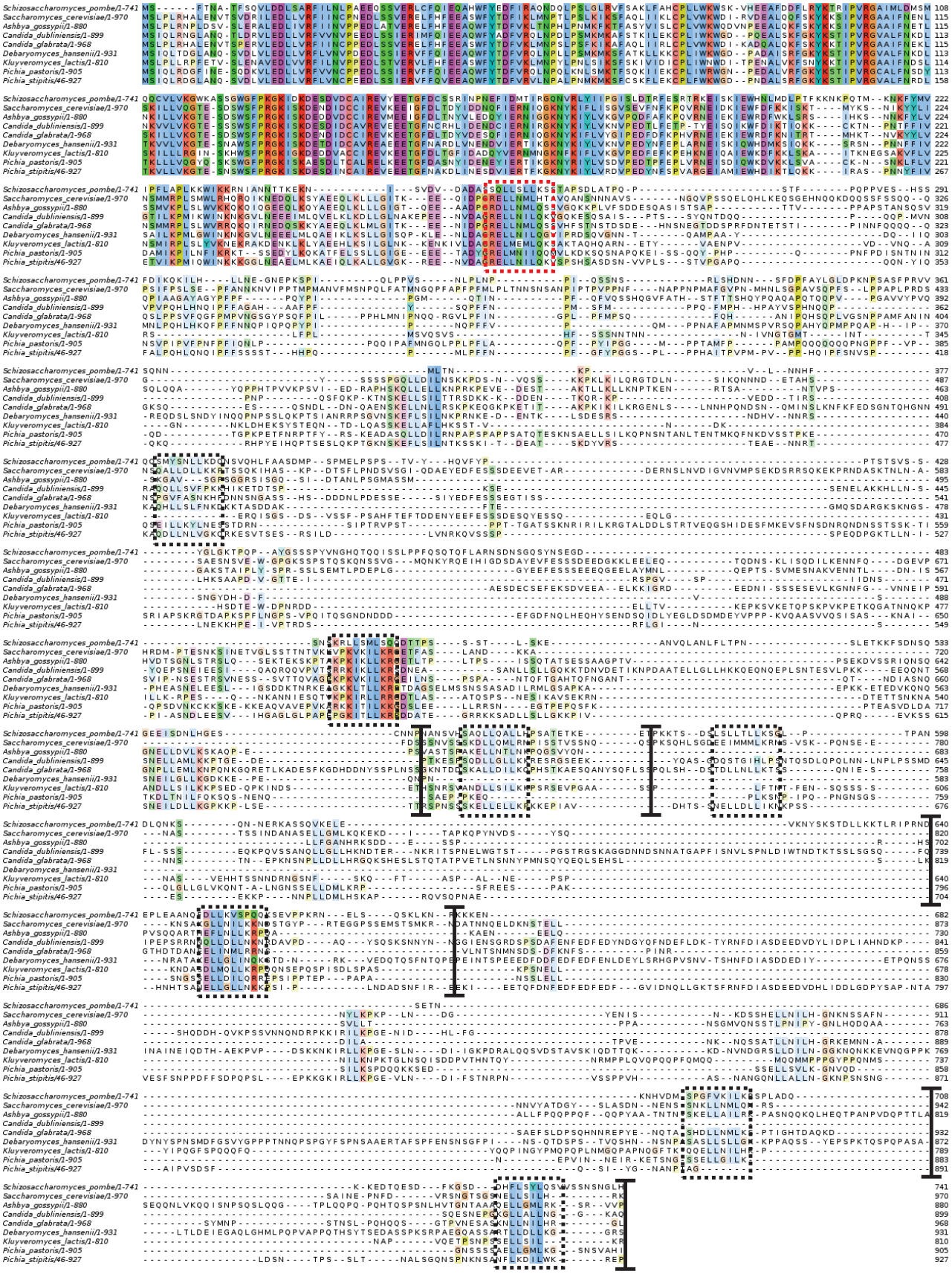

Figure S5: Sequence alignment of yeast Dcp2

Sequence alignment of Dcp2 from different yeast species. Amino acids are colored according to conservation. Note the highly conserved regulatory and catalytic domains. The first LSm interaction motif (HLM-1) is enclosed in a red dashed box. The conserved motifs in the C-terminal part of Dcp2 are in black dashed boxes. The boundaries of the constructs used to probe for interactions are indicated with vertical lines and contain one putative LSm interaction motif each. The location and numbers of HLMs varies between different yeast species. Between HLM-1 and the Dcp2 catalytic domain a potential HLM is absent in *S. pombe*. Additional HLMs might be present in the disordered Dcp2 C-terminal region from other yeast species.

Figure S6

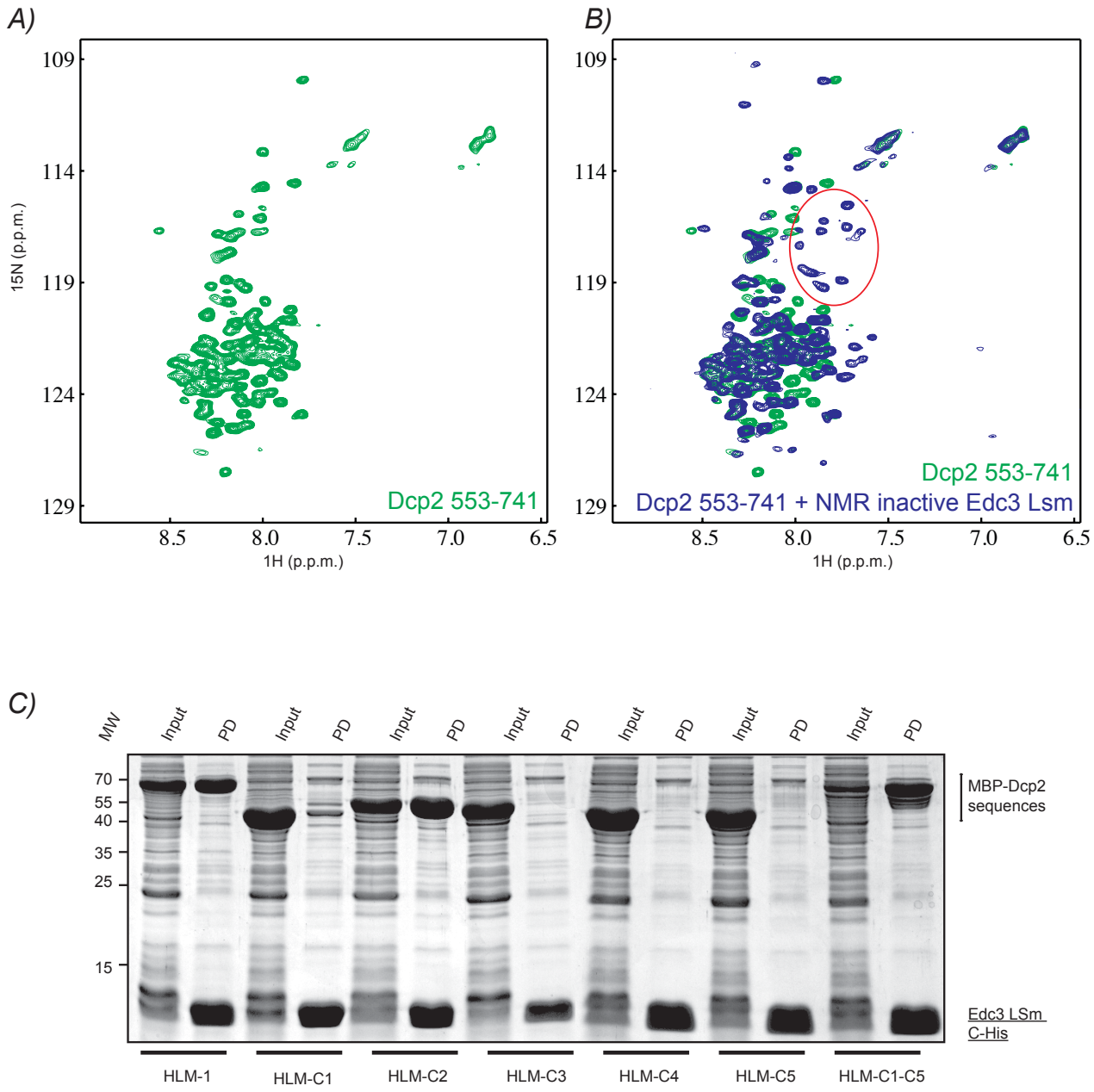

Figure S6: The disordered Dcp2 C-terminus interacts with Edc3

A. Spectrum of Dcp2 residues 553-741 (HLM-C1-C5; green). The lack of chemical shift dispersion indicates the disordered nature of the Dcp2 C-terminal extension.

B. Spectrum of Dcp2 residues 553-741 without (green, as in A) and with the Edc3 LSm domain (blue). The increase in chemical shift dispersion and the appearance of new resonances (e.g. red circle) indicates the formation of secondary structure upon the complex formation between the Dcp2 C-terminal tail and the NMR inactive Edc3 LSm domain. The Edc3 LSm domain is in ten fold molar excess compared to the Dcp2 C-terminus, such that most of the potential LSm

interaction motifs (HLM-C1 to HLM-C5) are bound to Edc3. The formation of the HLM-1 helix in Dcp2 upon the interaction with Edc3 is shown in Figure S2.

C. As Figure 3B, however, not only the pull-down (PD), but also the input is shown. In all experiments, MBP-HLM proteins were present in the soluble fraction. Only the HLM-1, HLM-C1, HLM-C2 and HLM-C1-C5 sequences co-purified with the Edc3 LSm domain.

Figure S7

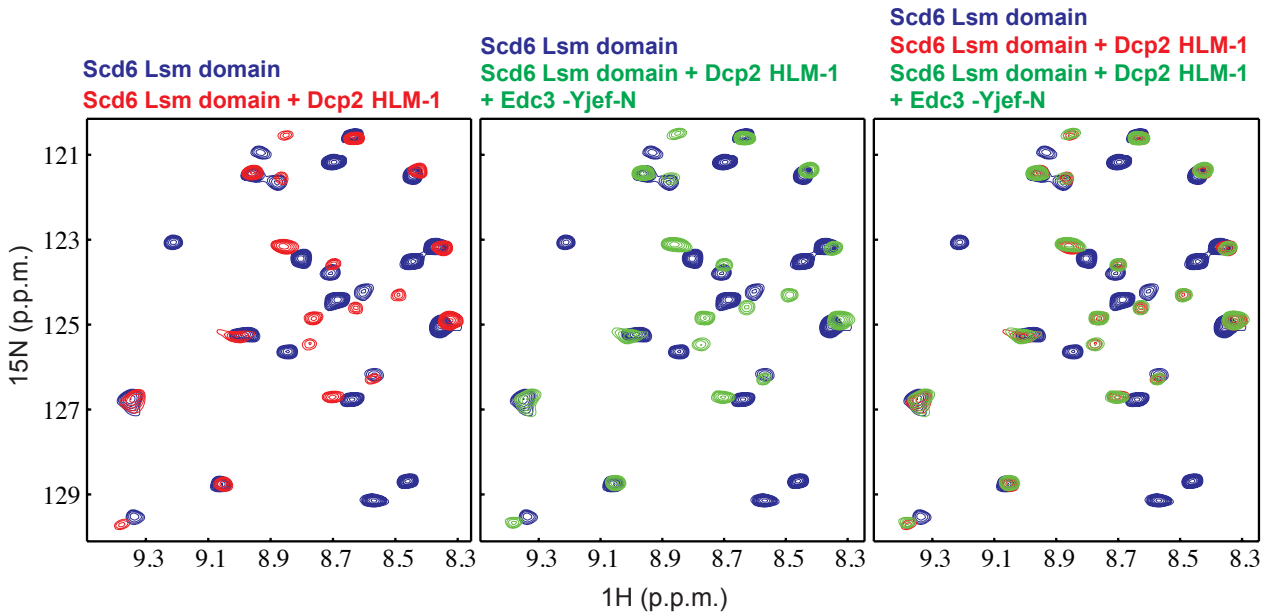

Figure S7: The Edc3 Yjef-N domain does not compete with Scd6:Dcp2-HLM-1 comlpex formation

Left: Spectrum of ^{15}N labeled Scd6 LSm domain free (0.1 mM, blue) and in complex with unlabeled Dcp2 HLM-1 (0.4 mM, red) (see also Figure 4B, left top in the main text).

Middle: Spectrum of ^{15}N labeled Scd6 LSm domain free (0.1 mM, blue) and a spectrum of a mixture of ^{15}N labeled Scd6 LSm domain (0.1 mM), Dcp2 HLM-1 (0.4 mM) and Edc3 Yjef-N domain (0.4 mM) (green spectrum).

Right: Overlay of the spectra shown in the left and middle. The red (Scd6 + Dcp2 HLM-1) and green (Scd6 + Dcp2 HLM-1 + Edc3 Yjef-N) spectra are identical. This shows that the Edc3 Yjef-N domain does not release Dcp2 HLM-1 from Scd6, as opposed to the Edc3 LSm domain that competes with the Scd6 LSm domain for binding to Dcp2 (Figure 4C).

Figure S8

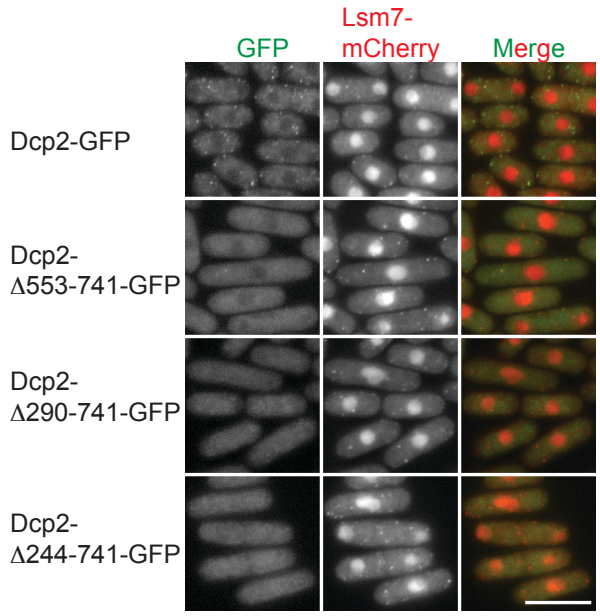
GFP
Lsm7-mCherry
Merge
Dcp2-GFP
Dcp2-Δ553-741-GFP
Dcp2-Δ290-741-GFP
Dcp2-Δ244-741-GFP

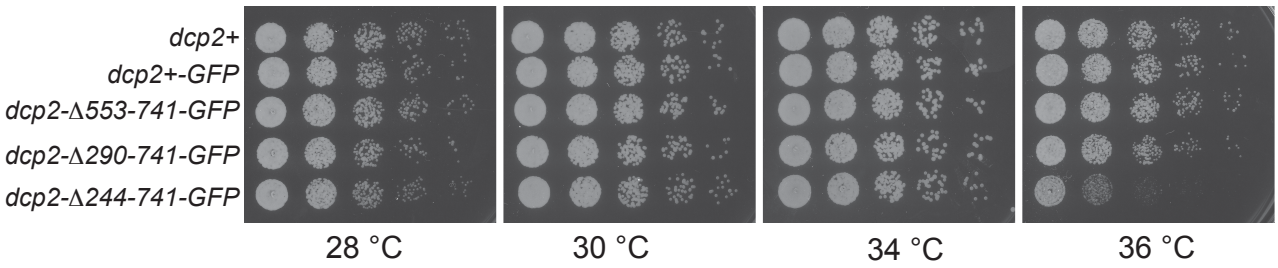
dcp2+
dcp2+-GFP
dcp2-Δ553-741-GFP
dcp2-Δ290-741-GFP
dcp2-Δ244-741-GFP
28 °C
30 °C
34 °C
36 °C

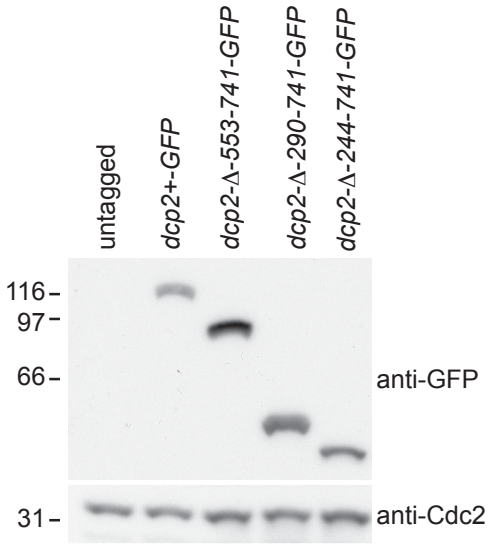
untagged
dcp2+-GFP
dcp2-Δ-553-741-GFP
dcp2-Δ-290-741-GFP
dcp2-Δ-244-741-GFP
116
97
66
anti-GFP
31
anti-Cdc2

Figure S8: Functional characterization of C-terminal Dcp2 truncations *in vivo*

A. Fluorescence micrographs of *S. pombe* strains expressing *dcp2+-GFP* or truncated versions thereof in combination with *lsm7+-mCherry*. While the localization of the truncated Dcp2-GFP proteins to P-bodies is abolished, Lsm7 is still enriched in these cytoplasmic foci. The nuclear staining of Lsm7 reflects its additional function as a member of the LSm2-8 complex that is an integral part of the U6 SnRNP. All images were scaled and processed in the same way. The length of the scale bar corresponds to 10 μm.

B. Growth test of different yeast strains expressing *dcp2+*(untagged), *dcp2+-GFP*, *dcp2-Δ553–741*, *dcp2-Δ290–741*, or *dcp2-Δ244–741*. Upon deletion of all HLMs (*dcp2-Δ244-741*), growth defects are observed at higher temperature indicating that the mutant protein no longer exhibits full functionality.

C. Immunoblotting for the cellular abundance of the different Dcp2-GFP versions. *S. pombe* cell extracts from the indicated strains were separated by SDS-PAGE and immunoblotted. Dcp2-GFP and its truncated forms were detected using an anti-GFP antibody. Cdc2 served as a loading control. The abundance of the truncated proteins was not reduced compared to the wild type protein.

Figure S9

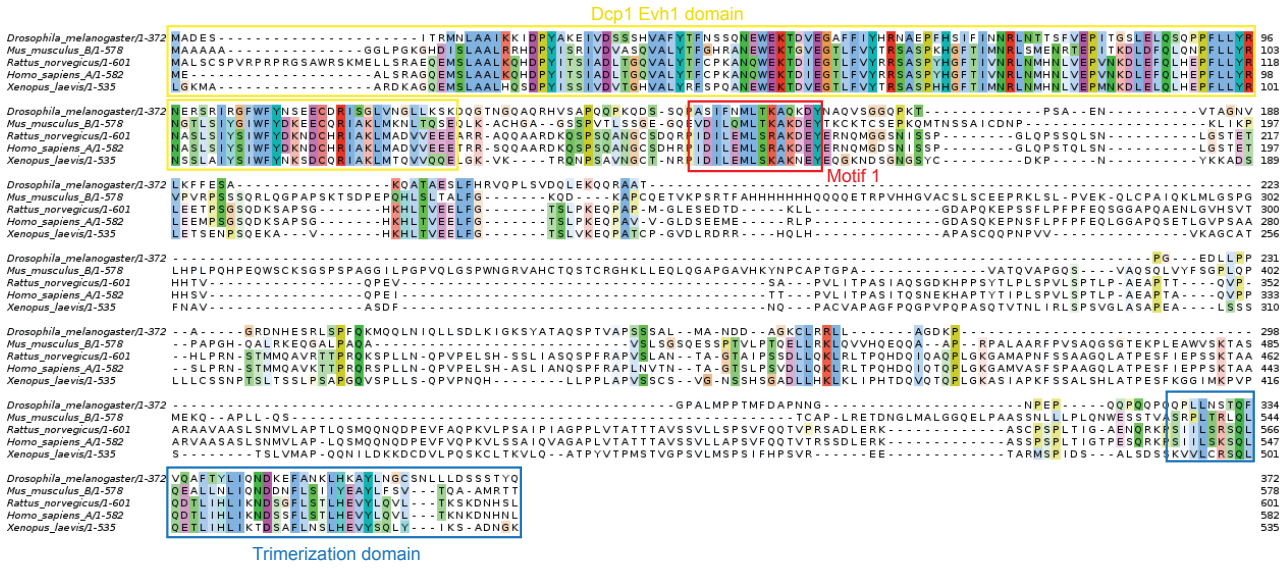

Figure S9: Dcp1 sequence alignment of metazoa

Alignment of the Dcp1 sequences from metazoa. The Evh1 and trimerization domains are boxed in yellow and blue, respectively. The motif I sequence (metazoan HLM) is indicated with a red box.

Table S1: Structural statistics

Table S1A: Edc3 LSm domain structure[1]

A. Structural statistics		
R.M.S.D from distance restraints (Å)[2]	SA	$\langle SA \rangle_r$
all (356)	0.030 ± 0.001	0.030
intra-residue (55)[9]	0.009± 0.007	0.015
inter-residue sequential (102)	0.025 ± 0.002	0.024
medium range (27)	0.041± 0.002	0.040
long range (141)	0.036± 0.001	0.036
hbond (28)	0.022 ± 0.004	0.031
R.M.S.D from dihedral restraints (deg) (188)[10]	0.07 ± 0.008	0.06
H-bond restraints average (Å/deg)[3] (24)	2.09 ± 0.22/ 20.2± 8.9	2.0 ± 0.20 / 18.76 ± 9.0
H-bond restraints min-max (Å/deg)[3]	1.75-2.58/ 8.19-44.91	1.68-2.59/ 9.37-44.12
Deviations from ideal covalent geometry		
Bonds (Å*10^{-3})	4.68 ± 0.001	4.78
Angles (deg.)	0.58± 0.003	0.584
Impropers (deg)	1.15 ± 0.04	1.16
Structure quality indicators[4]		
Ramachandran Map regions (%)	87.9/ 21.1/ 0.0	87.0/ 13.0/ 0.0

B. Atomic R.M.S. differences (Å)[5]				
	SA vs $\langle SA \rangle$		SA vs $\langle SA \rangle_r$	
	Backbone	All	Backbone	All
Secondary Structure[6]	0.26 ± 0.13	0.71± 0.09	0.44± 0.13	1.00 ± 0.11
$\langle SA \rangle$ vs $\langle SA \rangle_r$[7]	0.36	0.80		

See Table S1B for the legend.

Table S1B: Edc3 LSm domain: Dcp2 complex[1]

A. Structural statistics

R.M.S.D from distance restraints (Å)[2]	SA	$<SA>_r$
all (437)	0.031 ± 0.001	0.031
intra-residue (66)[9]	0.005± 0.006	0.007
inter-residue sequential (128)	0.029 ± 0.001	0.030
medium range (41)	0.046± 0.002	0.048
long range (158)[8]	0.033± 0.001	0.033
hbond (44)	0.036 ± 0.002	0.039
R.M.S.D from dihedral restraints (deg) (216)[10]	0.12 ± 0.003	0.11
H-bond restraints average (Å/deg)[3] (44)	2.15 ± 0.20/ 19.8± 8.4	2.1 ± 0.19 / 19.42 ± 9.1
H-bond restraints min-max (Å/deg)[3]	1.83-2.58/ 3.92-42.16	1.82-2.43/ 0.8-42.35
Deviations from ideal covalent geometry		
Bonds ($Å*10^{-3}$)	4.52 ± 0.001	4.55
Angles (deg.)	0.609± 0.005	0.606
Impropers (deg)	1.13 ± 0.03	1.08
Structure quality indicators[4]		
Ramachandran Map regions (%)	90.8/ 8.9/ 0.3	89.7 / 10.3 / 0.0

B. Atomic R.M.S. differences (Å)[5]

	SA vs <SA>		SA vs $<SA>_r$	
	Backbone	All	Backbone	All
Secondary Structure[6]	0.54 ± 0.14	0.84± 0.11	0.68± 0.21	1.09 ± 0.16
<SA> vs $<SA>_r$[7]	0.44	0.76		

[1] Structures are labeled as follows: SA, the set of 19/ 21 (structure of the free/ Dcp2 complexed Edc3 LSm domain) final simulated annealing structures; <SA>, the mean structure calculated by averaging the coordinates of SA structures after fitting over secondary structure elements; $<SA>_r$, the structure obtained by regularising the mean structure under experimental restraints.

[2] Numbers in brackets indicate the number of restraints of each type.

[3] Hydrogen bonds were restrained by treating them as pseudo-covalent bonds (see Materials and Methods). The average and minimum/maximum for distances and acceptor antecedent angles are stated for restrained hydrogen bonds.

[4] Percentages are for residues in favoured/allowed/outlier regions of the Ramachandran map.

[5] Based on heavy atoms superimpositions.

[6] Defined as residues V3-L58 / V3-L58; A254-S267 (structure of the free/ Dcp2 complexed Edc3 LSm domain)

[7] RMS difference for superimposition over ordered residues.

[8] 22 of which are intermolecular.

[9] Intra-residual contacts that were used to define dihedral angles were not used in the structure calculations and are not included here.

[10] Includes backbone dihedral restraints derived from TALOS (Cornilescu et al, 1999) and sidechain dihedral restraints derived from intra-residual NOE contacts and HNHB data.

Table S1C: Individual proteins in the Edc3 LSm domain: Dcp2 complex[1]

A. Structural statistics

R.M.S.D from distance restraints (Å)[2]	SA_{Edc3}	SA_{Dcp2}
all (388/49)	0.032 ± 0.001	0.013 ± 0.002
intra-residue (56/10)[7]	0.007± 0.006	0.000± 0.000
inter-residue sequential (111/17)	0.028 ± 0.001	0.020 ± 0.003
medium range (33/8)	0.039± 0.003	0.011± 0.004
long range (158/0)	0.036± 0.001	-
Hbond (30/14)	0.041 ± 0.003	0.003 ± 0.002
R.M.S.D from dihedral restraints (deg) (186/30)[8]	0.12 ± 0.005	0.01 ± 0.001
H-bond restraints average (Å/deg)[3] (30/14)	2.13 ± 0.20/ 19.8± 8.1	2.17 ± 0.28 / 15.82 ± 7.7
H-bond restraints min-max (Å/deg)[3]	1.81-2.55/ 4.74-42.46	1.80-2.53/ 7.21-24.80
Structure quality indicators		
Ramachandran Map regions (%)[4]	89.3 / 10.7/ 0.0	95.9 / 2.4 / 1.7

B. Atomic R.M.S. differences (Å)[5]

	SA vs <SA>		SA vs <SA>	
	Backbone	All	Backbone	All
Secondary Structure[6]	0.27 ± 0.05	0.68± 0.09	0.77± 0.21	1.13 ± 0.19

[1] Structures are labeled as follows: SA, the set of 21 final simulated annealing structures; <SA>, the mean structure calculated by averaging the coordinates of SA structures after fitting over secondary structure elements, for the Edc3 protein and the Dcp2 peptide, respectively.

[2] Numbers in brackets indicate the number of restraints of each type. Intra-residual contacts that were used to define dihedral angles were not used in the structure calculations and are not included here.

[3] Hydrogen bonds were restrained by treating them as pseudo-covalent bonds (see Materials and Methods). The average and minimum/maximum for distances and acceptor antecedent angles are stated for restrained hydrogen bonds.

[4] Percentages are for residues in favoured/allowed/outlier regions of the Ramachandran map.

[5] Based on heavy atoms superimpositions.

[6] Defined as residues V3-L58 (Edc3); A254-S267 (Dcp2)

[7] Intra-residual contacts that were used to define dihedral angles were not used in the structure calculations and are not included here.

[8] Includes backbone dihedral restraints derived from TALOS (Cornilescu et al, 1999) and sidechain dihedral restraints derived from intra-residual NOE contacts and HNHB data.

Table S2: Expression constructs used in this study

#	Protein/ Protein complex	Residues	Solubility/ Purification tag
1	Edc3	1-121	N-His_6-TEV
2	Edc3	1-94	Untagged
3	Dcp1:Dcp2	1-127 (Dcp1), 1-95 (Dcp2)	N-His_6-TEV (Dcp1)
4	Dcp1:Dcp2	1-127 (Dcp1), 1-254 (Dcp2)	N-His_6-TEV (Dcp1)
5	Dcp1:Dcp2	1-127 (Dcp1), 1-266 (Dcp2)	N-His_6-TEV (Dcp1)
6	Edc3	1-94	N-His_6-TEV
7	Dcp2	242-291 (HLM-1)	N-His_6-MBP-TEV
8	Dcp2	553-741 (HLM-C1-C5)	N-His_6-MBP-TEV
9	Dcp2	553-576 (HLM-C1)	N-His_6-MBP-TEV
10	Dcp2	577-640 (HLM-C2)	N-His_6-MBP-TEV
11	Dcp2	641-678 (HLM-C3)	N-His_6-MBP-TEV
12	Dcp2	679-708 (HLM-C4)	N-His_6-MBP-TEV
13	Dcp2	709-741 (HLM-C5)	N-His_6-MBP-TEV
14	Control	-	N-His_6-MBP-TEV
15	Dcp1:Dcp2	1-127 (Dcp1), 1-289 (Dcp2)	N-His_6-TEV (Dcp1)
16	Edc3	195-454	N-His_6-TEV
17	Edc3	1-454	N-His_6-TEV
18	Scd6	1-86	C-His_6
19	Scd6	1-86	N-His_6-TEV
20	Dcp1:Dcp2	1-127 (Dcp1), 1-243 (Dcp2)	N-His_6-TEV (Dcp1)
21	Dcp1:Dcp2 L260A, L264A	1-127 (Dcp1), 1-289 (Dcp2) 2L2A	N-His_6-TEV (Dcp1)
22	Edc3 *D.m.*	1-101	N-NusA-His_6-TEV
23	Dcp1 *D.m.*	148-169	N-His_6-MBP-TEV
24	Dcp2 L260A	242-291	N-His_6-MBP-TEV
25	Dcp2 L264A	242-291	N-His_6-MBP-TEV
26	Dcp2	96-266	N-His_6-TEV
27	Dcp2	553-741	N-His_6-TEV
28	Edc3	1-94	C-His_6
29	Dcp2	242-291 (HLM-1)	N-MBP-TEV
30	Dcp2	553-741 (HLM-C1-C5)	N-MBP-TEV
31	Dcp2	553-576 (HLM-C1)	N-MBP-TEV
32	Dcp2	577-640 (HLM-C2)	N-MBP-TEV
33	Dcp2	641-678 (HLM-C3)	N-MBP-TEV
34	Dcp2	679-708 (HLM-C4)	N-MBP-TEV
35	Dcp2	709-741 (HLM-C5)	N-MBP-TEV
36	Dcp2	96-291	N-MBP-TEV

Table S3: NMR Samples for the structure determination

#	Protein/ Protein complex	Constructs	Labeling	Concentration (mM)
1	Edc3 LSm	1	^{15}N	0.9
2	Edc3 LSm	1	$^{15}N/^{13}C$	0.8
3	Edc3 LSm: Dcp2 HLM-1	2+7	^{15}N	1.2
4	Edc3 LSm: Dcp2 HLM-1	2+7	$^{15}N/^{13}C$	1.4

Table S4: Yeast strains used in this study

Figure 6a		
RS002	*h-*	*leu1 ade6-M216 dcp2+-GFP<<kanR dcp1+-mCherry<<natR*
RS003	*h+*	*leu1 ade6-M216 dcp2-Δ553-741-GFP<<kanR dcp1+-mCherry<<natR*
RS008	*h-*	*leu1 ade6-M210 dcp2-Δ290-741-GFP<<kanR dcp1+-mCherry<<natR*
RS011	*h-*	*leu1 ade6-M216 dcp2-Δ244-741-GFP<<kanR dcp1+-mCherry<<natR*
Figure 6b		
RS001	*h+*	*leu1 ade6-M216 dcp2+-GFP<<kanR edc3+-mCherry<<natR*
RS013	*h+*	*leu1 ade6-M210 dcp2-Δ553-741-GFP<<kanR edc3+-mCherry<<natR*
RS006	*h+*	*leu1 ade6-M210 dcp2-Δ290-741-GFP<<kanR edc3+-mCherry<<natR*
RS009	*h+*	*leu1 ade6-M216 dcp2-Δ244-741-GFP<<kanR edc3+-mCherry<<natR*
Figure S8a		
RS016	*h+*	*leu1 ade6-M210 dcp2+-GFP<<kanR lsm7+-mCherry<<natR*
RS014	*h+*	*leu1 ade6-M216 dcp2-Δ553-741-GFP<<kanR lsm7+-mCherry<<natR*
RS007	*h-*	*leu1 ade6-M216 dcp2-Δ290-741-GFP<<kanR lsm7+-mCherry<<natR*
RS010	*h-*	*leu1 ade6-M216 dcp2-Δ244-741-GFP<<kanR lsm7+-mCherry<<natR*
Figure S8b and c		
JY333	*h-*	*leu1 ade6-M216*
RS015	*h-*	*leu1 ade6-M216 dcp2+-GFP<<kanR*
RS012	*h-*	*leu1 ade6-M216 dcp2-Δ553-741-GFP<<kanR*
RS005	*h-*	*leu1 ade6-M216 dcp2-Δ290-741-GFP<<kanR*
RS004	*h-*	*leu1 ade6-M216 dcp2-Δ244-741-GFP<<kanR*

Supplementary materials and methods

Protein purification

All proteins were purified using Ni affinity chromatography (50 mM sodium phosphate, pH 7.5, 10 mM imidazole, 150 mM NaCl; see main text). For the purification of protein complexes, only one of the components contained an affinity tag; untagged proteins were co-purified due to a tight intermolecular interaction with the tagged protein. Different proteins were co-expressed from a dicistronic vector (see Table S2) or by transforming two vectors (see Table S2) with different antibiotic resistance into *E. coli*. A potential excess of untagged protein was removed during the Ni affinity chromatography step. When applicable, the purification tag was removed with TEV protease. A potential excess of the tagged component was removed from the complex during the size exclusion chromatography purification step (Superdex 200 or Superdex 75, GE Healthcare in 25 mM HEPES buffer pH 7.3, 125 mM NaCl and 1 mM DTT).

Pull down experiments

For the pull-down experiments shown in Figure 1D cells that had overexpressed His_6-Dcp1:Dcp2 (constructs 3, 4 or 5) were supplemented with an equal amount of cells that had separately overexpressed untagged Edc3 LSm domain (construct 2). For the pull-down experiment shown in Figures 3B and S6, Edc3 1-94 C-His (construct 28) was co-expressed with the MBP-tagged Dcp2 (constructs 30-36). For the pull-down experiments shown in Figure 4A Scd6 C-His (construct 18) was co-expressed with Dcp2 (construct 36). In all cases, the soluble fraction of the cell lysate (input) was applied to Ni affinity resin and the eluted proteins were applied to SDS PAGE analysis and coomassie staining.

For the pull-down experiments shown in Figure 3D separately purified His_6-Dcp1:Dcp2 (construct 15; tag not removed), Dcp1:Dcp2 (construct 15; tag remoevd) and Edc3 (construct 6, 16 or 17; tag removed) were mixed at a 1:1:1 ratio (input). The mixture was applied to Ni affinity resin,

washed with 10 volume of column buffer and eluted with imidazole. The eluted protein complexes (PD) and the inputs were applied to SDS PAGE analysis and coomassie staining.

NMR titration experiments

NMR titration experiments shown in Figures 1E, 3C, 4B and S3A were performed by the addition of a five fold molar excess of NMR inactive (unlabeled) MBP-Dcp2 (constructs 7-14, 21 or 24-25, the His_6-MBP tag was not removed during the purification) to a 0.1 mM sample of separately purified ^{15}N labeled Edc3/ Scd6 (constructs 6 or 19; tag removed). The NMR titration experiment shown in Figure 7A was performed by the addition of a five fold molar excess of NMR inactive (unlabeled) MBP-Dcp1 motif 1 (construct 23) to a 0.1 mM sample of separately purified an ^{15}N labeled Edc3 (construct 22; tag removed). Addition of MPB (control) did not cause any chemical shift changes in the spectra of Edc3 or Scd6.

NMR titration experiments shown in Figure 4C and S7 were performed by addition of a four fold molar excess of unlabeled Dcp2 HLM-1 (construct 7; tag not removed) to 0.1 mM ^{15}N labeled Scd6 (construct 19; tag removed). Subsequently, unlabeled Edc3 LSm domain (construct 6; tag removed; Figure 4C) or unlabeled Edc3 Yjef-N domain (construct 16; tag removed; Figure S7) was added in a stepwise manner to a final concentration of 0.4 mM.

The NMR titration experiment show in Figure S3B was performed by the addition of NMR inactive (unlabeled) Edc3 (construct 6; tag removed) to separately purified ^{15}N labeled Dcp2 96-266 (construct 26; tag removed).

The NMR titration experiment shown in Figure S4 was performed by the addition of an equimolar amount of NMR inactive (unlabeled) Edc3 (construct 6; tag removed) to a 0.4 mM sample of separately purified $^{15}N^{2}H$ labeled Dcp1:Dcp2 (construct 15; tag removed), where Dcp1:Dcp2 deuteration was achieved by overexpression of the complex in D_2O based minimal medium. Prior to the NMR analysis, the backbone amides of the deuterated Dcp1:Dcp2 complex were re-protonated. To that extent, the 6M GuHCl denatured proteins were refolded by rapid

dilution into H_2O-based buffer containing 1.1 M guanidine, 55 mM Tris, 21 mM NaCl, and 88 mM KCl pH 8.2, followed by dialysis into size exclusion buffer.

The NMR titration experiment shown in Figures S6AB was performed by the addition of a ten fold molar excess of NMR inactive (unlabeled) Edc3 (construct 6; tag removed) to a 0.2 mM sample of separately purified ^{15}N labeled Dcp2 553-741 (construct 27; tag removed).

Figures displaying NMR spectra were prepared with NMRview (Johnson, 2004).

NMR sample preparation

NMR samples containing the Edc3 LSm domain were prepared using an N-terminally His_6-tagged version of the protein (construct 1; tag removed). The NMR samples of the Edc3 LSm domain Dcp2 complex were obtained from the co-expression of untagged Edc3-LSm (construct 2) domain and an His_6-MBP-TEV tagged peptide that corresponds to Dcp2 residues 242-291 (construct 7). The complex was purified using Ni affinity chromatography, where Edc3 co-purified with Dcp2 due to the very tight interaction between the two proteins. The His_6-MBP tag was cleaved from Dcp2 using TEV protease and removed from the Edc3:Dcp2 complex using a second Ni affinity chromatography step. A potential excess of Edc3 was removed from the complex during the first Ni-affinity step, a potential excess of Dcp2 was removed from the complex during the size exclusion chromatography purification step. The purified Edc3 LSm domain was in a 1:1 complex with Dcp2 as judged from NMR spectroscopy; no free Edc3 LSm domain or free Dcp2 was visible in any of the NMR spectra. The co-expression of Edc3 and Dcp2, resulted in a complex were both components were labeled with NMR active nuclei. Based on the backbone assignment and on an NMR sample that was labeled only in Edc3 (Figure 1E), resonances from Edc3 and Dcp2 could be distinguished. Due to the relatively small size of the complex there was no overlap between Edc3 and Dcp2 amide resonances. Filtered NMR experiments were not required to distinguish between intra- and intermolecular NOE restraints, due to the asymmetric nature of the complex and the low

extend of signal overlap in the NOE spectra. The elevated pH of the NMR sample (7.3) and the higher temperature during the measurements (303 K) resulted in the almost complete disappearance of the amide resonances of unstructured regions of the complex. This is due to the fast exchange rates of the labile amide protons with the bulk solvent.

NMR structure determination

NMR spectra were processed with the software provided by the spectrometer manufacturer (Topspin 2.1) or with the NMRPipe/ NMRDraw software suit (Delaglio et al, 1995). Spectra were analyzed using Sparky (T. D. Goddard and D. G. Kneller, SPARKY 3, University of California, San Francisco) and NMRView (Johnson, 2004).

For both the free Edc3 LSm domain and the Edc3:LSm complex, the backbone sequential assignment was completed using HNCA, HNCACB, HNCO and HN(CA)CO experiments optimized for fast pulsing using the extended flip-back scheme (Diercks et al, 2005), in combination with an CC(CO)NH-TOCSY experiment. Side-chain assignments were completed using 3D-CC(CO)NH-TOCSY and 3D-CCH-TOCSY spectra. Proton-proton distances were recorded on a ^{15}N-labeled sample (sample 1 or 3) using 3D-^{15}N-HSQC-NOESY (HNH-NOESY) and 3D-^{15}N-HSQC-NOESY-^{15}N-HSQC (NNH-NOESY) spectra and on a ^{15}N^{13}C-labeled sample (sample 2 or 4) using 3D-^{13}C-HSQC-NOESY (HCH-NOESY), 3D-^{13}C-HSQC-NOESY-^{13}C-HSQC (CCH-NOESY) and 3D-^{13}C-HSQC-NOESY-^{15}N-HSQC (CNH-NOESY) spectra (Diercks et al, 1999). Aromatic contacts were observed in ^{15}N-filtered 2D-NOESY spectra.

The χ1 angle and the stereospecific assignment of Hβ protons was determined based on an HNHB experiment (Archer et al, 1991) and relative NOE intensities of the intra-residual HN-Hβ1, HN-Hβ2 , Hα-Hβ1 and Hα-Hβ2 crosspeaks (Wagner et al, 1987) in 3D HNH-, HCH- and CCH-NOESY spectra. For valine residues the χ1 angle was determined based on the HNHB experiment and relative NOE intensities of intra-residual HN-Hβ, HN-Hγ1 , HN-Hγ2 and Hα-Hβ, Hα-Hγ1 , Hα-Hγ2 crosspeaks in 3D HNH-, HCH- and CCH-NOESY spectra. This can also

provide the stereospecific assignment of the methyl groups. For isoleucine and threonine residues the χ1 angle was determined based on the HNHB experiment and relative NOE intensities of the intra-residual HN-Hβ, HN-Hγ2 and Hα-Hβ, Hα-Hγ2 crosspeaks in 3D HNH-, HCH- and CCH-NOESY spectra. For leucine residues the χ2 angle was determined based on relative intra-residual NOE intensities of the Hα-Hδ1, Hα-Hδ2 , Hβ1–Hδ1, Hβ1–Hδ2, Hβ2–Hδ1 and Hβ2–Hδ2 cross-peaks in 3D HCH- and CCH-NOESY spectra. This can also provide the stereospecific assignment for the methyl groups. For isoleucine residues the χ2 angle was determined based on relative intraresidual NOE intensities of the Hα-Hδ1, Hγ2-Hδ1 , Hβ–Hδ1, Hα-Hγ11, Hγ2-Hγ11 , Hβ–Hγ11, Hα-Hγ12, Hγ2-Hγ12 and Hβ–Hγ12 crosspeaks in 3D HCH- and CCH-NOESY spectra. This can also provide the stereospecific assignment for the methylene γ protons. The determined χ1 and χ2 angles were used in the structure calculations. To that extend, the corresponding dihedral angle was restrained to +60 (+/- 30), -60 (+/- 30) or 180 (+/- 30) degrees depending on the rotameric state. The inter-residual NOE distances that were used to define the χ2 angle were not used as distance restraints in the structures calculations to avoid the use of redundant information.

Secondary chemical shift information derived from TALOS (Cornilescu et al, 1999) was used to generate backbone conformational restraints. NOESY cross peak intensities were scaled to the corresponding HSQC intensities and converted into four classes of distance restraints with upper distances of 2.7, 3.2, 4.0 and 5.0 Å, respectively. Lower distance restraints with a minimum distance of 3.2 Å were included for absent and very weak sequential HN-HN NOE contacts. Lower distance restraints with a minimum distance of 2.7 Å were applied for weak or medium intensity sequential and intraresidue HN-Hα NOE crosspeaks. Pseudoatoms allowances (using r^{-6} averaging) were added for methyl groups and non stereo-specifically assigned methylene groups.

Hydrogen bond restraints were applied for residues in secondary structure elements where donor-acceptor pairs were consistently identified in the calculations and where the typical NOE patterns were observed. The H-bonds were treated as covalent bonds between the amide proton and the carbonyl oxygen as described in (Truffault et al, 2001). In X-PLOR, these additional bonds were added to the molecular structure through the PATCH statement. To ensure proper hydrogen bond geometry, the bond length was weakly (14 kcal/mol per $Å^2$) restrained to 2.12 Å, whereas the bond angle was weakly (4 kcal/mol per rad^2) restraint to 0 degrees. It should be noted that force constants used are designed to be very weak compared to other restraints. In addition, an NOE distance restraint between the amide proton and the carbonyl oxygen was applied with a lower bound of 1.9 Å and an upper bound of 2.6 Å that prevents the hydrogen bond from being unrealistically short or long.

Structures were calculated with XPLOR (NIH version 2.9.3)(Schwieters et al, 2006; Schwieters et al, 2003) using a three-stage simulated annealing protocol. During the structure refinement, we compare experimental NOE strips (derived from HNH-, NNH-, HCH-, CCH- and CNH-NOESY spectra) with back-calculated NOE strips. The back-calculation was performed using in house written software that makes use of the full relaxation matrix (to include effects of spin diffusion) and the current structural model. This procedure allows us to identify potential inconsistencies between the data and the model that were due to wrongly assigned resonances, wrongly assigned NOE contact or wrongly determined rotameric states. These potential errors were then corrected in a novel round of structure refinement until no more inconsistencies were present. It should be noted that the large number of NOESY spectra we recorded (that resolves potential spectral overlap) and the back-calculation of the NOESY spectra (taking spin diffusion into account) are fundamental for this procedure to function properly.

Ensembles of 50 structures were calculated and a final set of 19 (Edc3 LSm domain) / 21 (Edc3:Dcp2 complex) was selected based on the basis of lowest restraint violations. For both

ensembles an average structure was calculated and regularized. Structural statistics are presented in Tables S1A, S1B and S1C).

S. pombe strain construction and imaging

Fission yeast strains used in this study are listed in Supplementary Table 4. Truncations and tagging of endogenous *dcp2+* with GFP and tagging of *dcp1+*, *edc3+* and *lsm7+* with mCherry (Shaner et al, 2004) were performed using the PCR-based gene targeting method for *S. pombe* (Bahler et al, 1998). For imaging, cells were grown at 30 °C to logarithmic growth phase in sterile filtered Edinburgh minimal medium (Moreno et al, 1991) containing the necessary supplements. Images were acquired at room temperature under identical imaging conditions using a 63x/ 1.4 oil objective on a Zeiss Axio Imager microscope coupled to a charged-coupled device camera. Images were processed with MetaMorph software (Molecular Devices Corporation).

S. pombe growth test

Serial dilution growth tests were performed by growing cells at 30 °C to logarithmic growth phase in liquid YEA (yeast extract containing adenine sulfate) medium (Moreno et al, 1991) and spotting a 1:5 serial dilution onto YEA plates containing Phloxin B plates (2 mg/mL, Sigma-Aldrich).

S. pombe cell extracts, SDS-PAGE and immunoblotting

Cells were grown in liquid YEA medium at 30 °C to logarithmic growth phase. $5*10^8$ cells were harvested and sequentially washed with 1 mL ice-cold 20 % trichloroacetic acid and 1mL 1M TRIS (unadjusted pH). Pellets were resuspended in 200 µL 2x SDS buffer (125 mM TRIS pH 6.8, 4 % SDS, 0.01 % bromophenol blue, 20 % glycerole, 200 mM DTT). Samples were boiled and subjected to a beat-beating procedure using a volume of 1200 µL acid-washed glass beads (Sigma, G8772) and the Bio101 FastPrep FP120 Homogenizer (three times 5 m/s for 40 s). Samples were

separated from beads by centrifugation and boiled again. Volumes corresponding to $2*10^6$ cells were subjected to SDS-PAGE. Proteins were blotted onto a PVDF membrane (Immobilon-P, Millipore) and detected by mouse anti-GFP (Roche, 11814460001) or rabbit anti-Cdc2 (Santa Cruz, SC-53). Secondary antibodies were anti-mouse and anti-rabbit HRP-conjugates respectively (Dianova, 115-035-003 and 111-035-003) and were detected using chemiluminescence.

Supplementary references

Archer SJ, Ikura M, Torchia DA, Bax A (1991) An alternative 3D-NMR technique for correlating backbone N-15 with side-chain H-beta-resonances in larger proteins. *J Magn Reson* **95:** 636-641

Bahler J, Wu JQ, Longtine MS, Shah NG, McKenzie A, 3rd, Steever AB, Wach A, Philippsen P, Pringle JR (1998) Heterologous modules for efficient and versatile PCR-based gene targeting in Schizosaccharomyces pombe. *Yeast* **14:** 943-951

Cornilescu G, Delaglio F, Bax A (1999) Protein backbone angle restraints from searching a database for chemical shift and sequence homology. *J Biomol NMR* **13:** 289-302

Delaglio F, Grzesiek S, Vuister GW, Zhu G, Pfeifer J, Bax A (1995) NMRPipe: a multidimensional spectral processing system based on UNIX pipes. *J Biomol NMR* **6:** 277-293

Diercks T, Coles M, Kessler H (1999) An efficient strategy for assignment of cross-peaks in 3D heteronuclear NOESY experiments. *J Biomol NMR* **15:** 177-180

Diercks T, Daniels M, Kaptein R (2005) Extended flip-back schemes for sensitivity enhancement in multidimensional HSQC-type out-and-back experiments. *J Biomol NMR* **33:** 243-259

Johnson BA (2004) Using NMRView to visualize and analyze the NMR spectra of macromolecules. *Methods Mol Biol* **278:** 313-352

Moreno S, Klar A, Nurse P (1991) Molecular genetic analysis of fission yeast Schizosaccharomyces pombe. *Methods Enzymol* **194:** 795-823

Schwieters CD, Kuszewski JJ, Clore GM (2006) Using Xplor-NIH for NMR molecular structure determination. *Progress in Nuclear Magnetic Resonance Spectroscopy* **48:** 47-62

Schwieters CD, Kuszewski JJ, Tjandra N, Clore GM (2003) The Xplor-NIH NMR molecular structure determination package. *J Magn Reson* **160:** 65-73

Shaner NC, Campbell RE, Steinbach PA, Giepmans BN, Palmer AE, Tsien RY (2004) Improved monomeric red, orange and yellow fluorescent proteins derived from Discosoma sp. red fluorescent protein. *Nat Biotechnol* **22:** 1567-1572

Truffault V, Coles M, Diercks T, Abelmann K, Eberhardt S, Luttgen H, Bacher A, Kessler H (2001) The solution structure of the N-terminal domain of riboflavin synthase. *J Mol Biol* **309:** 949-960

Wagner G, Braun W, Havel TF, Schaumann T, Go N, Wuthrich K (1987) Protein structures in solution by nuclear magnetic resonance and distance geometry. The polypeptide fold of the basic pancreatic trypsin inhibitor determined using two different algorithms, DISGEO and DISMAN. *J Mol Biol* **196:** 611-639